Statistical Properties of the Radiation Belt Seed Population

A.J. Boyd,[1] H.E. Spence,[1], C.-L. Huang[1], G. D. Reeves[2,3], D. N. Baker[4], D.L. Turner[5], S. G. Claudepierre,[5] J. F. Fennell[5], J. B. Blake[5], Y.Y. Shprits[6,7]

Corresponding author: Alexander J. Boyd, Institute for the Study of Earth, Oceans, and Space, University of New Hampshire, Durham, NH 03824, USA. (a.j.boyd@unh.edu)

[1]Institute for the Study of Earth, Oceans, and Space, University of New Hampshire, Durham, New Hampshire, USA.

[2]Space Science and Applications, Los Alamos National Lab, Los Alamos, New Mexico, USA.

[3]New Mexico Consortium, Los Alamos, New Mexico, USA.

[4]Laboratory for Atmospheric and Space Physics, University of Colorado, Boulder, Colorado, USA.

This article has been accepted for publication and undergone full peer review but has not been through the copyediting, typesetting, pagination and proofreading process, which may lead to differences between this version and the Version of Record. Please cite this article as doi: 10.1002/2016JA022652

Abstract. We present a statistical analysis of phase space density data from the first 26 months of the Van Allen Probes mission. In particular we investigate the relationship between the 10s-100s keV seed electrons and >1 MeV core radiation belt electron population. Using a cross correlation analysis, we find that the seed and core populations are well correlated with a coefficient of ≈ 0.73 with a time lag of 10-15 hours. We present evidence of a seed population threshold that is necessary for subsequent acceleration. The depth of penetration of the seed population determines the inner boundary of the acceleration process. However, we show that an enhanced seed population alone is not enough to produce acceleration in the higher energies, implying that the seed population of 100s of keV electrons is only one of several conditions required for MeV electron radiation belt acceleration.

[5]Space Sciences Department, The Aerospace Corporation, El Segundo, California, USA.

[6]Department of Earth, Planetary, and Space Sciences, University of California, Los Angeles, California, USA.

[7]Massachusetts Institute of Technology, Cambridge, Massachusetts, USA.

1. Introduction

The Earth's Van Allen radiation belts are some of the most dynamic regions in the inner magnetosphere. Understanding radiation belt dynamics is particularly important because the radiation belts contain high energy (>1 MeV) 'killer' electrons which are capable of severely damaging satellites [*Baker*, 2002]. *Reeves et al.* [2003] showed that the response of the radiation belt varies greatly for different geomagnetic storms. The response of the belts to an individual event depends on the balance of source and loss processes [e.g *Reeves et al.*, 2003; *Turner et al.*, 2014]. These source processes fall into two broad categories: 1) radial transport and 2) local acceleration. Radial transport involves moving particles from larger L into the inner magnetosphere. Through conservation of the first invariant, the particles are accelerated as they move inward. This process can also be enhanced by interaction with Ultra Low Frequency (ULF) waves [*Rostoker et al.*, 1998; *O'Brien et al.*, 2001; *Mann et al.*, 2004; *Shprits et al.*, 2008a]. The other process, local acceleration, has been shown to produce large, rapid enhancements in the radiation belts is local acceleration [e.g. *Reeves et al.*, 2013; *Baker et al.*, 2014a]. In particular, wave-particle interactions with VLF chorus waves have been shown to be particularly effective in accelerating electrons up to radiation belt energies [*Horne and Thorne*, 1998; *Summers et al.*, 2002; *Horne et al.*, 2005; *Thorne et al.*, 2005; *Summers et al.*, 2007]. While much of the focus in the acceleration process is on the high energy (>0.5 MeV) core electron population, the lower energy seed and source populations (defined below) interact with these waves and play key roles in the acceleration process.

The local acceleration process begins with the source population. These few-10s keV electrons, which are brought into the inner magnetosphere by substorm injections and enhanced global convection are capable of producing waves such as whistler-mode chorus [*Thorne et al.*, 2013]. These substorm injections also carry the 10s-100s keV seed electrons. These particles are able to be accelerated by the waves up to the relativistic energies seen in the radiation belt [*Baker et al.*, 1998]. This process, and the importance of the seed population has been both modeled and observed for several major enhancement events [e.g. *Thorne et al.*, 2013; *Li et al.*, 2014; *Tu et al.*, 2014; *Shprits et al.*, 2008b]. In addition, *Jaynes et al.* [2015] has shown that when either the seed and source population are absent, acceleration in the outer belt shuts down, despite otherwise favorable solar wind conditions.

While it is clear that the seed population is important to radiation belt acceleration, the exact relationship between the seed and core populations is less clear. *Li et al.* [2005] and *Turner and Li* [2008] analyzed daily-averaged fluxes at geosynchronous orbit over a five year-time period. They found that when a time lag was applied, the 10s-100s keV population fluxes were well correlated with the >1 MeV electron fluxes. However, since these observations were at geosynchronous orbit, they were not able to see the acceleration process itself, as it was happening in the heart of the radiation belt. In this study, we examine both the seed and core populations inside of the radiation belt over a long time period to see exactly how these two populations interact to produce radiation belt acceleration.

2. Data

The dual Van Allen Probes spacecraft were launched on August 30, 2012 with a comprehensive suite of instruments to study the fields, waves and particles within Earth's radiation belts [*Mauk et al.*, 2014]. For this study we used data from the Relativistic Electron Proton Telescope (REPT) [*Baker et al.*, 2014b], which measures high energy (1-20 MeV) electrons, and the Magnetic Electron-Ion Spectrometer (MagEIS) [*Blake et al.*, 2014] which measures low and medium energy (∼20-4000 keV) energetic electrons. Both of these instruments are part of the Energetic Particle, Composition, and Thermal (ECT) plasma instrument suite [*Spence et al.*, 2013]. These particle measurements, together with the magnetic field measurements from the Electric and Magnetic Field Instrument Suite and Integrated Science (EMFISIS) [*Kletzing et al.*, 2013] were used to calculate phase space density (PSD) for the Van Allen Probes mission from launch through the end of 2014.

To calculate the PSD, we followed the method laid out in *Boyd et al.* [2014]. Pitch angle resolved fluxes from MagEIS and REPT along with the magnetic field data from EMFISIS were used to calculate PSD as a function of the three adiabatic invariants μ, K and L*. *Tsyganenko and Sitnov* [2005] was used as the global magnetic field model for these calculations. Using the phase space density at fixed 2nd and 3rd invariant, we focused on how phase space density evolved as a function of 1st invariant μ. In particular, we investigated three distinct electron populations at different values. These populations are the seed population, which we define to be $\mu \approx 150$ MeV/G (∼200 keV at L*=5); the core population ($\mu \approx 1000$ MeV/G; ∼1 MeV at L*=5); and the ultra-relativistic population ($\mu \approx 4000$ MeV/G; ∼2.5 MeV at L*=5).

Our goal of this study was to use these data-sets to investigate two questions: 1) What correlations exist between these populations and what are the relevant acceleration timescales? and 2) What conditions in the seed population lead to enhancements in the core and ultra-relativistic populations?

3. Correlations and Timing

To investigate their correlations, we examined the phase space density of the seed, core and ultra-relativistic populations for a period of 26 months between October 2012 and December 2014. These observations are shown in Figure 1. For this time period, we restricted our attention to those particles that are mirroring relatively close to the magnetic equator(K=0.11 $R_{\mathrm{E}}G^{1/2}$) and well into the outer radiation belt ($\mathrm{L}^* = 5$). Figure 1 illustrates that each of these populations behave very differently and have different characteristic timescales. The seed population varies rapidly, with sharp increases on the timescale of hours. The core population varies less dynamically and follows a pattern of rapid increases followed by slow decay. The ultra-relativistic population follows a similar pattern to the core population, possessing even less dynamism. Despite these differences, there are many events, such as the 8-9 October 2012 event and the 17 March 2013 event, which elicit a coordinated response in all three of the populations, demonstrating that these populations are sometimes strongly correlated.

To understand these connections, we next quantify the properties of such events. Since the seed population is believed to play a key role in the acceleration process, we focused on enhancement events in the core ($\mu = 1000$ MeV/G) electrons. Similar to *Reeves et al.* [2003], we required enhancement events to meet the following criteria:

1. The core population must increase by at least a factor of 2.

2. The enhancement must be isolated, with no other events within ±48 hours.

3. There must be no data gaps of more than 10 hours during the event.

Implementing these criteria with second invariant K=0.11 $R_E G^{1/2}$ and L* = 5 gave 34 enhancement events over the 26-month period. These K and L* values were chosen since they represent the smallest K value continuously observed by the Van Allen Probes and the typical L* where the peak fluxes are observed. Although we did not place a requirement on of any geomagnetic indices, the events represent an equal mixture of quiet periods and storm-times, with 17 of the 34 events having a minimum Dst $\geq$ -40nT. In addition, all 34 of the events are associated with an elevated Auroral Electrojet (AE) index. Table 1 shows a summary of these events, and they are marked with gray triangles in Figure 1.

Our first goal was to investigate the correlation between the different electron populations. Following *Li et al.* [2005] and *Turner and Li* [2008], we implemented the technique of cross correlations. Since the observations of the Van Allen Probes at fixed L* are non-uniform in time, we interpolate between measurements to get a uniform set of observations. Then, for a number of μ value steps between 200 and 3000 MeV/G, we calculated the linear correlation coefficient between that population and the 150 MeV/G seed population. We then applied a series of time lags between -2 and -48 hours to the seed population and repeated the calculation of the correlation coefficient. For each μ value, we recorded the time lag that gave the maximum correlation coefficient. Time-lags as a function of μ for three L* values, calculated using all 26 months of data, are shown in Panel A of Figure 2. Similarly, Panel B shows the correlation coefficient as a function of μ, calculated using the full dataset. Panels C and D show similar results using only

data for the 5 days leading up to the maximum core phase space density for each of the 34 enhancement events. Data for L*=5.5 is not shown for the active times, as the L* of Van Allen Probes apogee is often less than 5.5 for periods of strong geomagnetic activity. The shaded regions in panels A and C represent the range of time-lags at L*=5 where the correlation coefficient was within 1% of the maximum value. For the purposes of this study, we only consider the correlation to be significant if R $\geq$ 0.7. The lines in panels A and C are dashed when the maximum correlation coefficient goes below this threshold.

As shown in Figure 2, the core population has its maximum correlation at 10-15 hours with a correlation coefficient between 0.7 and 0.8. These results are consistent between L* = 4.5 and L* = 5.5, with marginally highest correlations at L*=5. The value of the coefficient is similar for the active times, but the maximum correlation time-lag is much shorter, with a maximum between 0-13 hours. These results agree with the findings of *Turner and Li* [2008], who performed a similar study using fluxes at geostationary orbit. For similar energies, *Turner and Li* [2008] found a similar correlation coefficient (0.8) and a larger time-lag (between -17 and -34 hours).

As shown in panels A and C, this correlation is only significant up to ≈800-1000 MeV/G. This indicates that while the seed population is well correlated with the core population not directly connected to the ultra relativistic population. However, when performing a similar analysis with respect to the 1000 MeV/G core population, we found that the core and ultra-relativistic populations were very well correlated, with R >0.8 up to 5000 MeV/G. These results are consistent with the stepwise acceleration processes described in *Boyd et al.* [2014], where the seed population is accelerated up to 1 MeV and then subsequent acceleration brings that population up to multi-MeV energies.

The correlation coefficients shown in Figure 2 give the average timing for all of the events, but the timing for individual events can vary greatly. Figure 3 shows the distribution of time lags for each of the enhancement events that meet the criteria described above for μ = 1000 MeV/G and μ = 4000 MeV/G. For the core population, in the majority of the events the maximum seed population PSD occurs <20 hours before the core, but there are several events with much longer timescales (>25 hours). Similarly, for the ultra-relativistic population, the maximum seed population occurs 25-35 hours earlier, but several of the events have much shorter or longer timescales. As shown in both panels, for all of the events, the seed population enhancement preceded the enhancement at higher energies.

4. Superposed Epoch Analysis

Our next focus was to investigate the seed population conditions that lead to radiation belt acceleration. Therefore, we needed to know what the seed population conditions were for each of the core enhancement events. We used superposed epoch analysis to investigate this. For each event, we used the L* where the largest enhancement was observed. As shown in Table 1, for more than half (18) of the events, this was at or near the Van Allen Probes apogee (L* >5.25), but several of the events featured enhancements inside of L* = 5. As shown in *Schiller et al.* [2014], PSD peaks are often found beyond the Van Allen Probes apogee. Therefore, while 7 of the events showed clear evidence of PSD peaks at low L*, it is possible more of the events had a peak at higher L*. The t=0 epoch time was defined to be at the maximum core population PSD for each event.

The results of this analysis are shown in Figure 4. The three panels show the ultra-relativistic, core and seed population PSDs respectively. In all panels, the median (thick

line) and the upper and lower quartiles are shown. The sequence of the acceleration process is shown clearly in Figure 4, with the seed population reaching its maximum first (t=-0.5-0.0), followed by the core population (t=0), and ultimately the ultra-relativistic population (t=1).

The initial conditions (difference between the upper and lower quartile values) for all three of the populations vary by about an order of magnitude. The final values for the core and ultra-relativistic populations vary by roughly the same amount. However, this is not the case for the seed population. All of the events end up with nearly the same number of seed electrons (to within a factor of 5). This is despite the fact that the initial conditions of the seed population varies by several orders of magnitude. Given that all of these events showed an enhancement in the core population, it is possible that this represents the minimum, or threshold value for the seed population. This value at 1×10^{-4} $(\frac{c}{cm \cdot MeV})^3$ is labeled in Figure 4.

5. Seed Population Threshold

The seed population threshold can also be investigated by looking at all seed population enhancements. Using a similar set of criteria to those used to identify the core enhancement events (i.e. 2x increase in seed population), we identified 97 events at L*=5 and 76 events at L*=4.5. For each of these seed population enhancements, we compared the maximum PSD value with the fractional change in the core population PSD in the following 48 hours. This comparison at L*=4.5 and L*=5, is shown in Figure 5. In both panels, the shaded region indicates where the max PSD is above the threshold from Figure 4. For all values of max seed PSD, there were many events that did not lead to core enhancements, so it is immediately clear that larger seed population values do not necessarily lead to

enhancements in the core population. However, all of the events that did lead to core enhancements (shown by the red markers) have maximum seed populations near or above 1×10^{-4} $(\frac{c}{cm \cdot MeV})^3$. This provides further evidence that this value represents a necessary threshold for the seed population in order to produce a core population enhancement.

As noted earlier, the superposed epoch shown in Figure 4 was done at the L* where the acceleration was taking place. It is plausible that the seed population plays a role in controlling the location of the acceleration for each event. To investigate this, for each event, we compared the minimum L* where the seed population was above the threshold value to the minimum L* (to within $\pm$ 0.25) where the core population increased by at least a factor of 2.

The relationship between the minimum L* at which the core acceleration takes place and minimum L* penetration of the seed population is shown in Figure 6. These values are very well correlated, with a linear correlation coefficient of 0.84. In addition, for nearly all of the events, to within L* $\pm$ 0.25, the enhanced seed population penetrates further inward than where the acceleration is observed. This suggests that the seed population forms an inner boundary. Only outside of this boundary are there are enough seed electrons to facilitate the acceleration process.

The majority of the time, when the seed population is above the threshold, there are enhancement events in the core population. Additionally, all of the core enhancement events seen in the 26-month interval were preceded by a seed population enhancement, indicating they are one key ingredient to core population enhancements. However, the seed population is only one part of the acceleration process. Without waves to accelerate the seed electrons, there would be no enhancements to the $>$ 1 MeV populations. For the

enhancement events described here, the VLF chorus observations are shown in Figure S1 in the supporting information.

As noted in Table 2 at L* = 5.5, the seed population is above the threshold value more than 70% of the time. This is consistent with the results of *Turner et al.* [2015], who found that seed electrons were enhanced in 87% of geomagnetic storms in the Van Allen Probes era. Even with an elevated seed population, continued chorus wave activity driven by substorm activity is needed to drive MeV electron enhancements [*Meredith et al.*, 2001, 2002]. In addition, these acceleration processes take place at the same time as loss processes. As shown in Table 2, there are many instances when loss processes overwhelm any acceleration taking place, or there is no acceleration seen in the higher energy populations. All of these results point to the fact that the seed population is a critical piece in a very delicate acceleration process. While an enhanced seed population is necessary, alone it is not sufficient for radiation belt acceleration.

6. Discussion

Beginning with the work of *Baker et al.* [1998], the seed population has been recognized as a key part of the acceleration process. While the seed population has been well studied for particular events, this paper represents one of the first statistical studies of the seed population in the radiation belts and how these properties relate to the variability in the core population. These results also show conclusively that there are distinct differences in the behavior of the core and ultra-relativistic populations, as proposed by *Shprits et al.* [2013]. The results presented here confirm the results of *Li et al.* [2005] and *Turner and Li* [2008], showing a strong correlation between the seed and MeV populations. However, we offer a considerable improvement on these previous results by examining phase space

density in the heart of the radiation belts rather than daily-averaged fluxes at geosynchronous orbit. First, Using phase space density allows for the removal of adiabatic effects and ensure that observed enhancements represent a real change in the particle population within the radiation belts. Second, the observations of the Van Allen Probes at low L-shells offer a better measurement of the acceleration timescales. This is particularly true during periods where local acceleration is active, as observations at geosynchronous will be delayed since the particles have to first radially diffuse outward.

As noted in *Turner and Li* [2008] and *Li et al.* [2005], in addition to local acceleration, radial transport processes can also explain the time-lags seen between the 100s keV and MeV electrons. This is due to the fact that lower energy electrons drift inward faster, so they are observed earlier. While it would be difficult, if not impossible, to completely separate the radial transport and local acceleration effects for each event, we note that, on average, we observe smaller time-lags than the studies at geosynchronous orbit. It is possible that some of this discrepancy can be attributed to differences in geomagnetic activity and ULF wave power between these periods. However, if radial transport were the dominant mechanism for most of these events, we would expect to see larger time-lags, as the particles take longer to drift into lower L-shells. Therefore, while radial transport is undoubtedly responsible for some of the results in this study, local acceleration likely plays an important role in most of the events, particularly those at lower L*.

We have also shown that the seed population is not strongly correlated with the ultra-relativistic population. One possible reason for this are loss processes, such as the interaction with electromagnetic ion cyclotron (EMIC) waves. Recent work from *Mourenas et al.* [2016] has shown that strong chorus wave activity, coupled with EMIC waves can lead to

strong losses in the ultra-relativistic electrons, limiting or overwhelming any enhancements that may be occurring at these energies.

The work presented here makes it clear that seed population plays a critical role in controlling both where and when core population enhancements will take place. All of the core enhancement events seen in this 26-month period were associated with seed population enhancements up to a particular level. This level likely represents a threshold value that the seed population must reach in order for the acceleration process to take hold. It is possible that this threshold represents a saturation point for these electrons in the inner magnetosphere. As shown in Figure 6, acceleration can only begin when a given L* is filled or saturated with seed electrons. It is probable that this saturation point is associated with the Kennel-Petschek limit. As described in *Kennel and Petschek* [1966], the fluxes of electrons of this energy range are subject to an upper limit imposed by pitch angle scattering via wave particle interactions.

For average strength magnetic field, at L*=5, μ=150 MeV/G corresponds to ∼230 keV. Therefore, a PSD value of 1×10^{-4} $(\frac{c}{cm \cdot MeV})^3$ will correspond to a flux of $1.04 \times 10^4 \frac{\#}{s \cdot sr \cdot cm^2 \cdot keV}$. From the values provided by *Schulz and Davidson* [1988] and *Summers et al.* [2009], the Kennel-Petschek differential limiting flux at this energy and L-value would be between $\sim 5 \times 10^3$ and $\sim 7 \times 10^4 \frac{\#}{s \cdot sr \cdot cm^2 \cdot keV}$, depending on the shape of the pitch angle distribution. We have shown that observations of these events are consistent with local acceleration by these same waves. Therefore, since these waves would be active during these periods, it is not surprising that this threshold is comparable with the Kennel-Petschek limit, and the seed population must be close to this saturation limit in order to produce an enhancement of MeV electrons.

However, as mentioned here, the seed population is only one part of the acceleration process. Our results show that large variability in the seed population leads to much smaller changes in the higher energies. In order to better understand the details of this process, future studies will also involve incorporating the source population along with chorus and ULF wave activity to investigate the other ingredients required for the acceleration process. In particular, recent work by *Ma et al.* [2016] has shown that the source population (and subsequent wave generation) can play an important role in the acceleration process, leading to enhancements of the seed population and strongly influencing the acceleration timescales. Finally, further investigation into the relationship between the seed population and geomagnetic indicies such as AE could yield useful results that could be useful for models and for the use of the seed population as a predictor of core population enhancements.

7. Conclusions

Here, we have investigated the statistical relationship between the radiation belt seed, core and ultra-relativistic populations using phase space density observations for the first 26 months of the Van Allen Probes mission. We have 3 main conclusions:

1. The seed population (150 MeV/G) is strongly correlated with the core population (1000 MeV/G), but is not directly connected to the ultra-relativistic population (4000 MeV/G).

2. The strongest correlation between the seed and core populations is at a 10-15 hour time lag. This time lag is smaller (0-13 hours) during enhancement events.

3. The seed population is subject to a threshold value or saturation limit that is a necessary condition for the enhancement of MeV electrons.

All of these conclusions are consistent with a step-wise acceleration picture where a 10s-100s keV seed population that is accelerated up to $\approx$ 1 MeV and then is subsequently accelerated up to multi-MeV energies. While this picture has been previously shown for individual events, this study shows that the seed population plays an important role in governing radiation belt dynamics.

Acknowledgments. This work was supported by RBSP-ECT funding provided by JHU/APL Contract No. 967399 under NASA's Prime Contract No. NAS5-01072. RBSP-ECT data is available at http:\\www.rbsp-ect.lanl.gov. EMFISIS data available at http:\\emfisis.physics.uiowa.edu.

References

Baker, D., X. Li, J. Blake, and S. Kanekal (1998), Strong electron acceleration in the Earth's magnetosphere, *Advances in Space Research*, *21*(4), 609–613, doi:10.1016/S0273-1177(97)00970-8.

Baker, D. N. (2002), How to Cope with Space Weather., *Science (New York, N.Y.)*, *297*(5586), 1486–7, doi:10.1126/science.1074956.

Baker, D. N., et al. (2014a), Gradual diffusion and punctuated phase space density enhancements of highly relativistic electrons: Van Allen Probes observations, *Geophysical Research Letters*, *41*(5), 1351–1358, doi:10.1002/2013GL058942.

Baker, D. N., et al. (2014b), The Relativistic Electron-Proton Telescope (REPT) Instrument on Board the Radiation Belt Storm Probes (RBSP) Spacecraft: Characterization of Earth's radiation belt high-energy particle populations, *The Van Allen Probes mission*, *179*(1-4), 337–381, doi:10.1007/978-1-4899-7433-4-11.

Blake, J. B., et al. (2014), The Magnetic Electron Ion Spectrometer (MagEIS) instruments aboard the Radiation Belt Storm Probes (RBSP) spacecraft, *The Van Allen Probes mission*, *9781489974*(1-4), 383–421, doi:10.1007/978-1-4899-7433-4-12.

Boyd, A. J., H. E. Spence, S. G. Claudepierre, J. F. Fennell, J. B. Blake, D. N. Baker, G. D. Reeves, and D. L. Turner (2014), Quantifying the radiation belt seed population in the 17 March 2013 electron acceleration event, *Geophysical Research Letters*, *41*(7), 2275–2281, doi:10.1002/2014GL059626.

Horne, R. B., and R. M. Thorne (1998), Potential waves for relativistic electron scattering and stochastic acceleration during magnetic storms, *Geophysical Research Letters*, *25*(15), 3011, doi:10.1029/98GL01002.

Horne, R. B., et al. (2005), Wave acceleration of electrons in the Van Allen radiation belts, *Nature*, *437*(7056), 227–230, doi:10.1038/nature03939.

Jaynes, A. N., et al. (2015), Source and seed populations for relativistic electrons: Their roles in radiation belt changes, *Journal of Geophysical Research*, *120*(9), 7240–7254, doi:10.1002/2015JA021234.

Kennel, C. F., and H. E. Petschek (1966), Limit on stably trapped particle fluxes., *Journal of Geophysical Research*, *71*(1), 1–28, doi:10.1029/JZ071i001p00001.

Kletzing, C. A., et al. (2013), The Electric and Magnetic Field Instrument suite and Integrated Science (EMFISIS) on RBSP, *The Van Allen Probes mission*, *179*(1), 127–181, doi:10.1007/978-1-4899-7433-4-5.

Li, W., et al. (2014), Radiation belt electron acceleration by chorus waves during the 17 March 2013 storm, *Journal of Geophysical Research: Space Physics*, *119*(6), 4681–4693, doi:10.1002/2014JA019945.

Li, X., D. N. Baker, M. Temerin, G. D. Reeves, R. H. Friedel, and C. Shen (2005), Energetic electrons, 50 keV to 6 MeV, at geosynchronous orbit: Their responses to solar wind variations, *Space Weather*, *3*(4), 1–10, doi:10.1029/2004SW000105.

Ma, Q., D. Mourenas, A. Artemyev, W. Li, R. M. Thorne, and J. Bortnik (2016), Strong enhancement of 10-100keV electron fluxes by combined effects of chorus waves and time domain structures, *Geophysical Research Letters*, *43*(10), 4683–4690, doi: 10.1002/2016GL069125.

Mann, I. R., T. P. O'Brien, and D. K. Milling (2004), Correlations between ULF wave power, solar wind speed, and relativistic electron flux in the magnetosphere: Solar cycle dependence, *Journal of Atmospheric and Solar-Terrestrial Physics*, *66*(2), 187–198, doi: 10.1016/j.jastp.2003.10.002.

Mauk, B. H., N. J. Fox, S. G. Kanekal, R. L. Kessel, D. G. Sibeck, and A. Ukhorskiy (2014), Science objectives and rationale for the Radiation Belt Storm Probes mission, *The Van Allen Probes mission*, *179*(1), 3–27, doi:10.1007/978-1-4899-7433-4-2.

Meredith, N. P., R. B. Horne, R. R. Anderson, and B. Horne (2001), Substorm dependence of chorus amplitudes: Implications for the acceleration of electrons to relativistic energies, *Journal of Geophysical Research*, *106*(A7), 13,165, doi:10.1029/2000JA900156.

Meredith, N. P., R. B. Horne, R. H. A. Iles, R. M. Thorne, D. Heynderickx, and R. R. Anderson (2002), Outer zone relativistic electron acceleration associated with substorm-enhanced whistler mode chorus, *Journal of Geophysical Research*, *107*(A7), 1144, doi: 10.1029/2001JA900146.

Mourenas, D., A. V. Artemyev, Q. Ma, O. V. Agapitov, and W. Li (2016), Fast dropouts of multi-MeV electrons due to combined effects of EMIC and whistler mode waves,

Geophysical Research Letters, *43*(9), 4155–4163, doi:10.1002/2016GL068921.

O'Brien, T. P., R. L. McPherron, D. Sornette, G. D. Reeves, R. Friedel, and H. J. Singer (2001), Which magnetic storms produce relativistic electrons at geosynchronous orbit?, *Journal of Geophysical Research*, *106*(A8), 15,533, doi:10.1029/2001JA000052.

Reeves, G. D., K. L. McAdams, R. H. W. Friedel, and T. P. O'Brien (2003), Acceleration and loss of relativistic electrons during geomagnetic storms, *Geophysical Research Letters*, *30*(10), doi:10.1029/2002GL016513.

Reeves, G. D., et al. (2013), Electron acceleration in the heart of the Van Allen radiation belts., *Science (New York, N.Y.)*, *341*(6149), 991–4, doi:10.1126/science.1237743.

Rostoker, G., S. Skone, and D. N. Baker (1998), On the origin of relativistic electrons in the magnetosphere associated with some geomagnetic storms, *Geophysical Research Letters*, *25*(19), 3701, doi:10.1029/98GL02801.

Schiller, Q., X. Li, L. Blum, W. Tu, D. L. Turner, and J. B. Blake (2014), A nonstorm time enhancement of relativistic electrons in the outer radiation belt, *Geophysical Research Letters*, *41*(1), 7–12, doi:10.1002/2013GL058485.

Schulz, M., and G. Davidson (1988), Limiting energy spectrum of an electron radiation belt, *Journal of Geophysical Research*, *93*(A1), 59–76, doi:10.1002/2014JA020250.

Shprits, Y. Y., S. R. Elkington, N. P. Meredith, and D. A. Subbotin (2008a), Review of modeling of losses and sources of relativistic electrons in the outer radiation belt I: Radial transport, *Journal of Atmospheric and Solar-Terrestrial Physics*, *70*(14), 1679–1693, doi:10.1016/j.jastp.2008.06.008.

Shprits, Y. Y., D. A. Subbotin, N. P. Meredith, and S. R. Elkington (2008b), Review of modeling of losses and sources of relativistic electrons in the outer radiation belt

II: Local acceleration and loss, *Journal of Atmospheric and Solar-Terrestrial Physics*, *70*(14), 1694–1713, doi:10.1016/j.jastp.2008.06.014.

Shprits, Y. Y., D. Subbotin, A. Drozdov, M. E. Usanova, A. Kellerman, K. Orlova, D. N. Baker, D. L. Turner, and K.-C. Kim (2013), Unusual stable trapping of the ultrarelativistic electrons in the Van Allen radiation belts, *Nature Physics*, *9*(11), 699–703, doi:10.1038/nphys2760.

Spence, H. E., et al. (2013), Science goals and overview of the Radiation Belt Storm Probes (RBSP) Energetic Particle, Composition, and Thermal Plasma (ECT) suite on NASA's Van Allen Probes mission, doi:10.1007/978-1-4899-7433-4-10.

Summers, D., C. Ma, N. P. Meredith, R. B. Horne, R. M. Thorne, D. Heynderickx, and R. R. Anderson (2002), Model of the energization of outer-zone electrons by whistler-mode chorus during the October 9, 1990 geomagnetic storm, *Geophysical Research Letters*, *29*(24), 2174, doi:10.1029/2002GL016039.

Summers, D., B. Ni, and N. P. Meredith (2007), Timescales for radiation belt electron acceleration and loss due to resonant wave-particle interactions: 2. Evaluation for VLF chorus, ELF hiss, and electromagnetic ion cyclotron waves, *Journal of Geophysical Research*, *112*(4), 1–21, doi:10.1029/2006JA011993.

Summers, D., R. Tang, and R. M. Thorne (2009), Limit on stably trapped particle fluxes in planetary magnetospheres, *Journal of Geophysical Research: Space Physics*, *114*(10), n/a–n/a, doi:10.1029/2009JA014428.

Thorne, R. M., T. P. O'Brien, Y. Y. Shprits, D. Summers, and R. B. Horne (2005), Timescale for MeV electron microburst loss during geomagnetic storms, *Journal of Geophysical Research*, *110*(A9), 9202, doi:10.1029/2004JA010882.

Thorne, R. M., et al. (2013), Rapid local acceleration of relativistic radiation-belt electrons by magnetospheric chorus, *Nature*, *504*(7480), 411–414, doi:10.1038/nature12889.

Tsyganenko, N. A., and M. I. Sitnov (2005), Modeling the dynamics of the inner magnetosphere during strong geomagnetic storms, *Journal of Geophysical Research*, *110*(A3), A03,208, doi:10.1029/2004JA010798.

Tu, W., G. S. Cunningham, Y. Chen, S. K. Morley, G. D. Reeves, J. B. Blake, D. N. Baker, and H. Spence (2014), Event-specific chorus wave and electron seed population models in DREAM3D using the Van Allen Probes, *Geophysical Research Letters*, *41*(5), 1359–1366, doi:10.1002/2013GL058819.

Turner, D. L., and X. Li (2008), Quantitative forecast of relativistic electron flux at geosynchronous orbit based on low-energy electron flux, *Space Weather*, *6*(5), 1–8, doi:10.1029/2007SW000354.

Turner, D. L., et al. (2014), On the cause and extent of outer radiation belt losses during the 30 September 2012 dropout event, *Journal of Geophysical Research*, *119*(3), 1530–1540, doi:10.1002/2013JA019446.

Turner, D. L., T. P. O'Brien, J. F. Fennell, S. G. Claudepierre, J. B. Blake, E. Kilpua, and H. Hietala (2015), The effects of geomagnetic storms on electrons in Earth's radiation belts, *Geophysical Research Letters*, pp. n/a–n/a, doi:10.1002/2015GL064747.

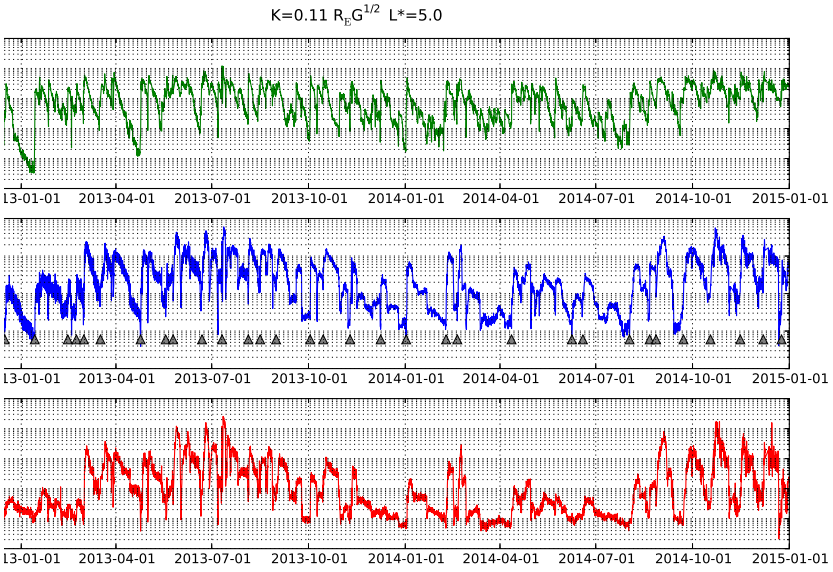

Figure 1. Overview of the phase space density for 3 different μ values: Seed (150 MeV/G), Core (1000 MeV/G) and Ultra-relativistic (4000 MeV/G) for a period from October 2012 through December 2014. All the data are for K=0.11 $R_{\mathrm{E}}G^{1/2}$ and L* = 5. The gray triangles in the core panel denote core enhancement events.

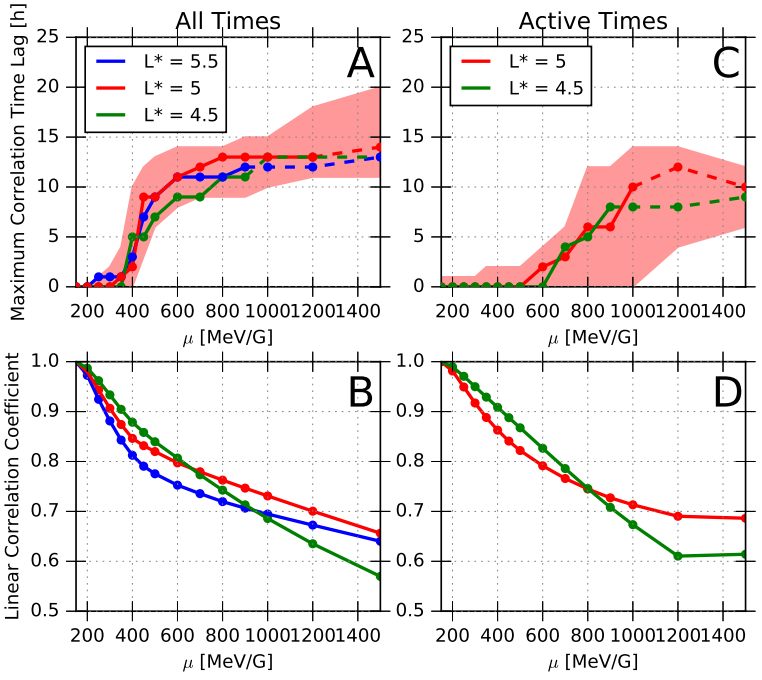

Figure 2. Results of the cross correlation analysis. Panels A and B show results with all 26 months of available data, panels C and D only includes results from within 5 days of a core enhancement event. Panels A and C show the time-lag that gives the maximum correlation coefficient with respect to the =100 MeV/G population as function of for 3 different L* values. Panels B and D show the correlation coefficient as a function of μ.

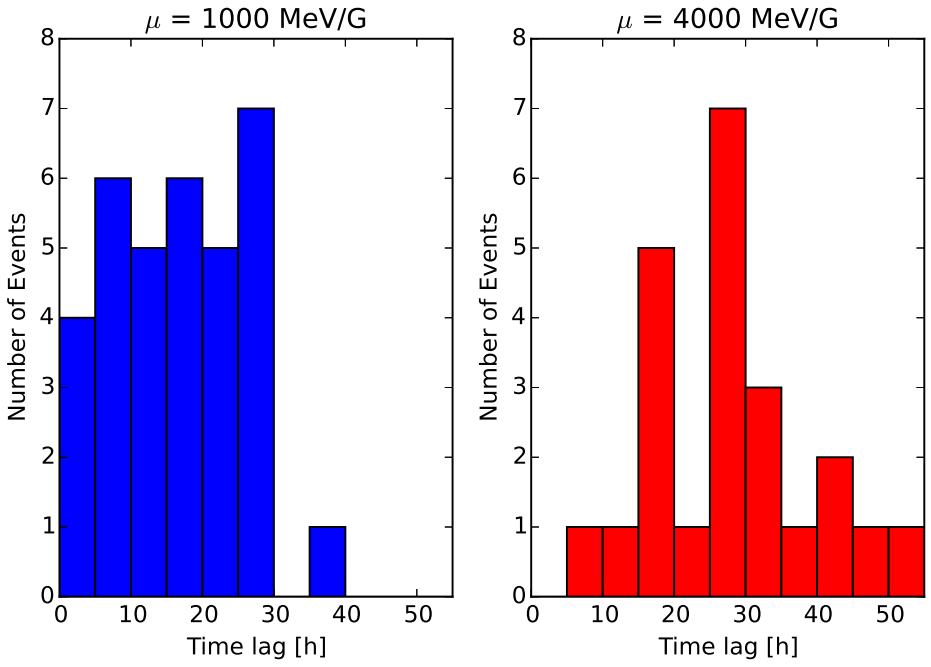

Figure 3. Distribution of time lags for all core enhancement events relative to the μ=150 MeV/G seed population. Left panel shows μ = 1000 MeV/G, right panel shows μ = 4000 MeV/G.

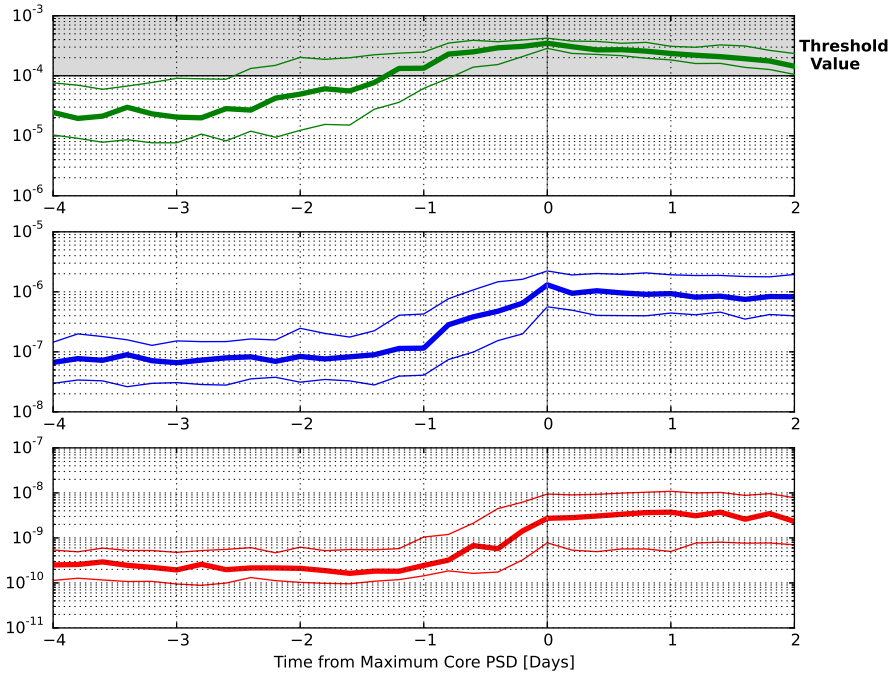

Figure 4. Superposed epoch analysis for all core enhancement events. Top panel shows the ultra-relativistic population($\mu = 4000$ MeV/G), the middle panel shows the core population ($\mu = 1000$ MeV/G) and the bottom panel shows the seed population ($\mu = 100$ MeV/G). In each panel, the thick line is the median, and the thinner lines the upper and lower quartiles. T=0 epoch time was taken to be the maximum core PSD for each event. Data for each event is taken at the L* where the largest core enhancement was observed. The apparent threshold value and/or saturation limit at 1×10^{-4} is marked on the seed population plot.

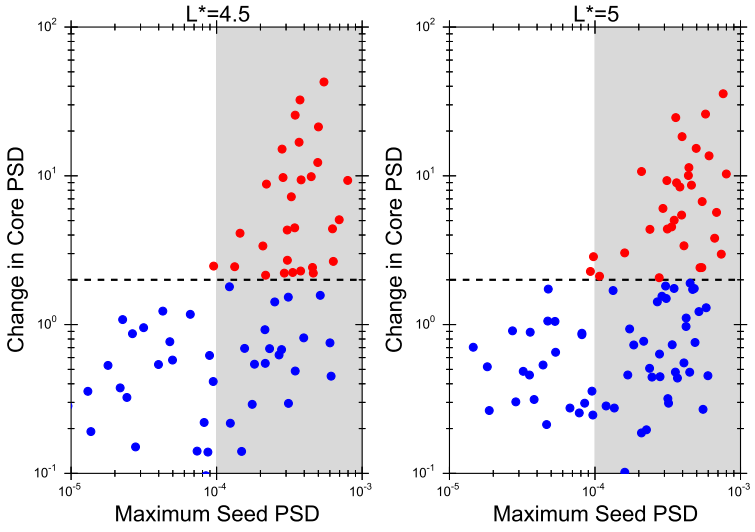

Figure 5. Comparison of the maximum seed PSD value and the fractional change in the core PSD for the following 48 hours for each seed population enhancement. Left panel shows data from L*=4.5, right panel shows L*=5. The horizontal dashed line marks where the core population increased by a factor of 2. Points above this value are shaded red. The shaded region shows where the maximum seed population PSD is above the threshold value and/or saturation limit of 1×10^{-4}

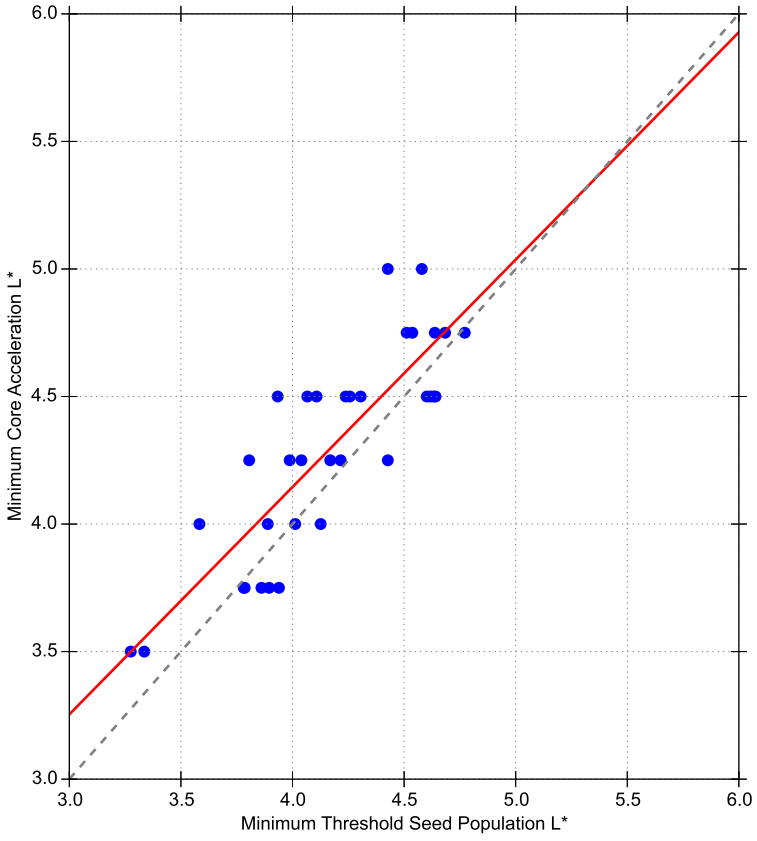

Figure 6. Relation between the minimum L* where the seed population is above the threshold value and/or saturation limit of 1×10^{-4} and the minimum L* where the core population was enhanced by at least a factor of 2. The red line is the best-fit line with a linear correlation of 0.84.

Table 1. Properties of the core enhancement events used in this study. Columns describe the date of the enhancement, the L* where the maximum enhancement is seen, The ratio of the maximum to minimum PSD, the ratio of average post-event PSD to pre-event PSD, whether the event had clear observations of PSD peaks, and the minimum Dst for the event.

Date	$L^*_{enhancement}$	Max/Min PSD	Post/Pre PSD	Clear PSD Peaks?	Min Dst [nT]
2012-10-09	4.2	472.1	232	Yes	-105
2012-11-15	4.5	92	19.3	Yes	-108
2012-12-18	Apogee	25.5	12.9	No	-27
2013-01-15	Apogee	34.4	24.5	No	-30
2013-02-15	Apogee	11.3	6.2	No	-36
2013-02-22	Apogee	41.6	8.6	No	-32
2013-03-02	5.0	166.4	21.9	No	-55
2013-03-18	4.2	148.2	22.8	Yes	-132
2013-04-27	5.0	343.4	36.2	No	-50
2013-05-19	4.5	75.2	9.1	Yes	-57
2013-05-28	4.5	17.1	16.7	No	-50
2013-06-24	5.0	114.2	13.4	No	-21
2013-07-10	4.7	13.6	20.8	No	-45
2013-08-04	4.7	200.5	9.4	Yes	-44
2013-08-16	Apogee	15.1	3.9	No	-35
2013-08-31	Apogee	38.9	5.5	No	-37
2013-10-02	5.0	49.4	37	No	-60
2013-10-14	Apogee	12.1	4.9	No	-43
2013-11-09	4.6	61.5	17.2	Yes	-81
2013-12-08	Apogee	28.8	5.7	No	-66
2014-01-01	Apogee	111.6	36.8	No	-40
2014-02-11	Apogee	116.9	72.5	No	-30
2014-02-21	Apogee	78.8	36.7	No	-116
2014-04-14	Apogee	44	26.5	No	-81
2014-06-09	Apogee	8.7	3.0	No	-38
2014-06-21	Apogee	14.5	5.0	No	-33
2014-08-05	Apogee	15.1	10.4	No	-18
2014-08-21	5.25	38	6.7	No	-32
2014-08-28	4.5	153.9	14.1	Yes	-80
2014-09-25	Apogee	99.9	44.9	No	-22
2014-10-19	5.0	29.8	24.5	No	-21
2014-11-17	Apogee	139.9	42.8	No	-50
2014-12-08	4.8	68.9	16.7	No	-24
2014-12-25	4.7	46.2	5.1	No	-38

Table 2. Statistics for core enhancements and the seed population threshold.

L*	Fraction of Time above Threshold	Total Events	Enhancement Events (%)	Acceleration, no Enhancement (%)	No Acceleration (%)
4	0.075	25	14 (56 %)	2 (8 %)	9 (36 %)
4.5	0.301	52	31 (59 %)	14 (26 %)	7 (13.5 %)
5	0.532	55	33 (60 %)	9 (16 %)	13 (24 %)
5.5	0.707	62	35 (56 %)	10 (16 %)	17 (27 %)